Multi-scale pattern with surface quasi crystal for wettability tuning

Sh. Golghasemi Sorkhabi, S. Ahmadi-Kandjani, F. Cousseau, S. Dabos-Seignon, M. Loumaigne, E. Ortyl, S. Zielinska, R. Barille

Multi-scale pattern with surface quasi crystal for wettability tuning

Sh. Golghasemi Sorkhabi,[1] S. Ahmadi-Kandjani,[2] F. Cousseau,[1] S. Dabos-Seignon,[1] M. Loumaigne,[1] E. Ortyl,[3] S. Zielinska,[3] and R. Barille[1]

[1] University of Angers MOLTECH-Anjou (UMR6200), Univ. Angers, CNRS, F-49045 Angers, (France)
[2] University of Tabriz/Research Institute for Applied Physics and Astronomy (RIAPA), University of Tabriz, Tabriz, (Iran)
[3] Wroclaw University of Technology] Department of Polymer Engineering and Technology, Wroclaw University of Technology, Faculty of Chemistry, 50-370 Wroclaw, (Poland)
Corresponding author: regis.barille@univ-angers.fr, matthieu.loumaigne@univ-angers.fr

Abtract

Fabrication and characterization of transparent and stretchable structures with multi-scale patterns on PDMS surfaces for a tunable superhydrophobicity is presented. The samples result in the transfer of photoinduced quasi-crystal structures of azopolymer-based thin films onto an elastomer. The quasi-crystal surface patterns have different complexities generated with superimposed multiple exposures. The obtained samples can be stretched or compressed. Periodic circular nanocavities as small as 500 nm could be obtained with their shapes changed by stretching. An elongation of more than 40% of the PDMS sample length could be obtained leading to a stretch of 6 mm. The surface stretching or compressing induced on the elastomer surface allows the size manipulation of nanocavities. An application of these surfaces is presented for a large control of the super-hydrophobicity. The wetting of these patterns is compared to the same surface pattern modified with metal nanoparticles obtained by a metal dewetting process where the roughness is increased. We show that in this case the hydrophobicity is higher, and the droplet is sticky on these surfaces leading to a rose-petal effect.

Keywords: surface quasi-crystal; super-hydrophobicity; rose-petal effect; stretchable nanocavities; photoinduced surface pattern; elastomeric stamp; azo-polymers

1. Introduction

Complex and engineered surface structures can manipulate light through physical effects, such as scattering, diffraction, and interference. Recently, it has been reported that micro/submicrometer surface relief structures provide wide applications in various optical devices, such as diffraction gratings [1, 2], microlens arrays [3, 4], or sensors [5]. These optical surfaces have a growing interest due to many new potential applications in photonics. Among all these surface structures, 2D quasi-crystal structures present a type of unconventional crystallographic structures possessing a long-range aperiodic order and a rotational symmetry [6]. Quasi-crystal structures laid out on surfaces of polymer thin films can be considered as a new type of engineered surfaces and could be used as novel multiscale patterns. Quasi-crystal structures with mesoscale range have been prepared through different methods like photolithography, using materials such as photoresist [7] or polymer-dispersed liquid crystal [8]. 2D surface relief quasi-crystals used as diffraction gratings with a tunable periodicity represent promising alternatives for a dynamic modulation of the beam directionality and steering [9]. The choice of a material, a low-cost process and an operational simplicity are challenging. The realization of spatial-modulated diffraction gratings remains a challenge, due to the limited strain tolerance of conventional materials. Quasi-crystal patterns on surfaces give rise to the control of well-ordered nano-cavities during the fabrication process. These cavities are very suitable for nanoparticle deposition in order to perform, for instance, single nanoparticle dark-field spectroscopy at low concentrations [10], and to create metamaterials [11] at higher concentrations. The fabrication of surface quasi-crystal structures on azopolymer films can be used as a new approach to further developments of the surface patterning technology based on the photo-driven mass migration scheme. The photofabrication of surface relief patterns on thin films of azobenzene-containing polymers has attracted a considerable attention [12]. Surface-relief gratings (SRGs) can be inscribed on azo polymer films upon irradiation with an interfering laser beam with a wavelength in the absorption band of the azopolymer at temperatures well below the glass transition temperatures (T_g) of the polymers.

Recently, quasi-crystal patterns have been prepared by double-beam multiple exposure technique using epoxy-based azopolymer as a processing material [13]. They have shown that quasi-crystal surface relief structures on azopolymer films can be inscribed by a suitable multiple exposure procedure. However, the surface patterns were characterized without any demonstrations of the possibilities to use the surface structure itself or to replicate them on other materials for further developments.

Azopolymer surfaces are not totally transparent and are not chemically inert. Here, we propose to adapt the duplication of the photoinduced azopolymer surface-relief gratings through a soft lithographic approach [14, 15], for the case of the quasi-crystal, in order to create a transparent, stretchable or compressible [16] and chemically inert surface, with tunable and ordered nanocavities with different complexities for further applications. Replications of a surface on a transparent material as PDMS with a high elasticity gives the ability to dynamically tune the surface properties of a material (such as wetting, adhesion, and friction) when a controlled movement is highly desirable for many future sensor applications.

These fabricated surfaces give us the opportunity to develop samples in the goal to achieve superhydrophobic surfaces with tunable water adhesions. Actually, many methods, such as surface ablation, polymer imprinting, surface photo-structuration have been utilized to fabricate different microstructures These techniques nowadays, suffer from intrinsic shortcomings such as high cost, complexity, and expensive mask fabrication. All of them are different of our proposed fabrication method and cannot be done simply at a low cost. We can cite different techniques of fabrication. For example, superhydrophobic surfaces with a tunable water adhesion [17], Robust omniphobic surfaces composed of polymeric mushroom-like microstructures [18] or hierarchically wrinkled polymer films [19] were fabricated. Holographic lithography for scalable optical gratings with hierarchical micro/nano structures was recently proposed [20]. The surfaces were replicated on PDMS. However, the patterns consist in surface gratings with different modulation depths as the one we can find in [21] with two spot diffracted patterns.

Moreover, most of the PDMS films are wrinkled films where the micro-scale surface roughness is regulated via a mechanical strain [22]. Recently, mechanical elongations were applied to a PDMS film with grooved surfaces along the directions parallel and perpendicular to the grooves, indicating deformation of topological morphology on the surface of the film [23] but the pattern was very simple consisting in unidirectional surface modulation. The measurement of the contact angle (CA) as a function of the stretch ration was measured [24]. A tunable and reversible anisotropic wetting behavior was observed. Silica nanoparticles deposited onto a rippled PDMS surface were also presented to generate a dual-scale roughness. Silica nanoparticles were patterned onto superhydrophobic surfaces demonstrating that a hierarchical surface with nanoparticles enhances the superhydrophobicity by both increasing the contact angle and delaying the Cassie-Wenzel transition [25]. The roughness at two or more length scales are known to be implicated as the cause of the Lotus or Petal effect [26, 27]. However, the nanoparticles were dip-coated with a non-homogeneous covering and the surface contains a simple micro-scale ripple pattern. Wells with 10-100 nm depths and a diameter on the order of micrometers were produced with a buckling instability on a polymer film. Silver nanoparticles and surface area of 6 cm^2 can be obtained. Ag nanoparticles were deposited at room temperature by dc sputtering but on a flat PDMS.

In this study, we combine all the previous characteristics of elastomeric surfaces with the fabrication of multiscale surfaces in the goal to test the possibility to change the anisotropic surface deformation with adjustable shaped nano-cavities acting as nano-wells with sub-micrometer dimensions. Quasi-crystal sample surfaces with nano and micro-scale topographies with a control over the roughness and the surface pattern can be used for the fabrication of tunable superhydrophobic surfaces with the aim to control the attachment or sliding of droplets. We present several complex quasi-crystal surfaces formed on azopolymer thin films with their elastomer (PDMS) replica. We demonstrate that the characterization of the PDMS replica surfaces leads to the same results as the measurements done by AFM on azopolymer thin films.

Finally, we integrate nanoparticles into the quasi-crystal system to generate a multi-scale roughness to promote the surface wetting and to switch from the Wenzel region to the Cassie-Baxter region in order to increase the flow resistance. The nanoparticles are directly fabricated on the surface by a metal-dewetting technique rarely used for optimized surface

modifications. We attempt to combine complex micro and nanostructures with nanoparticles directly fabricated on the quasi-crystal surface to create superhydrophobic surfaces. The wetting or the flow resistance is changed by tuning the topography of micro and nano-scaled quasi-crystal patterns using a mechanical strain of the elastomer surface. This experiment shows the interest in the development of this deformable surface quasi-crystal on elastomers to explore the dynamic switching of wetting behaviors. These results could lead to a broad range of engineering applications, such as anti-fouling materials, manipulation of cell growth direction and transport, SERS measurements or droplet manipulation.

2. METHODS

a. Azopolymer thin film preparation

Polymer thin films are made from a highly photoactive azobenzene derivative containing heterocyclic sulfonamide moieties, which has shown its huge capacity for surface patterning. The details of synthesis of 3-[4-[(E) - (4-[(2, 6-dimethyl- pyrimidin-4-yl)amino]sulfonylphenyl) diazenyl] phenyl-(methyl)amino]propyl2-methylacrylate are reported elsewhere [28]. Thin films were prepared by dissolving Azopolymer in THF (50 mg in 1 mL THF). The solution was filtered through 0.45 µm membrane and spin-coated on a pre-cleaned glass substrate. Prepared films were let in oven overnight at 60 °C to remove any residual solvent. The film thickness was determined by a Dektak Profilometer and was around 550 - 600nm. Molecular mass of the polymer determined by GPC was between 14000 and 19000 g/mol. The glass transition temperature (Tg) was 57 °C.

b. Inscription of Surface Relief Gratings

The inscription of the 2D quasi-crystal pattern is done by irradiation of azopolymer thin films with an interference pattern given by polarized laser beams. It leads to a reversible and controlled topographic modification of the polymer film surface, which results in the induction of a surface relief grating, in conjunction with the light interference pattern [29]. The process occurs readily at room temperature (well below the T_g of the amorphous polymers used) and it is believed that a large-scale photo-driven migration of polymer chains occurs during the SRG formation [30].
In a surface relief grating experiment, two beams interfere at an angle θ at the sample surface, giving rise to an SRG with period:

$$\lambda = \frac{\lambda}{2sin\theta} \quad (1)$$

where λ is the wavelength of the inscription light.
Microscopic surface relief gratings were inscribed onto the polymer films using a horizontally linearly polarized beam of a DPSS laser operating at a wavelength of λ = 473

nm. The beam was spatially filtered, collimated and then split by a beam splitter (BS), giving two beams with an equal intensity. The two beams, after reflecting from a mirror, were recombined to form an interference pattern and were incident on the sample stage. The exposure time for each grating was 5 - 10 minutes with a laser power of 0.7 W cm^{-2}. However, the higher numbers of gratings (for 8-fold and 16-fold quasi-crystal structures) needed a higher exposure time to reach a sufficient efficiency, which was controlled by the acquisition of a diffracted beam with a photodiode. After each irradiation, the sample was rotated by a calculated angle depending on the complexity of the surface structure required, and a new exposure was repeated on the same spot. The degree of rotation depends on the number of multiple exposures done on the sample. For 2, 4, 8, 16 exposures the degree of rotation is 90, 45, 22.5, 11.25 degrees, respectively. The sample was placed on a rotation holder, which did not suffer any transverse translational displacements.

c. PDMS replica of azo gratings

The Poly(dimethylsiloxane) (PDMS) prepolymer was purchased from Momentive (RTV 615). PDMS is a polymeric organo-silicon compound. It is optically transparent and does not allow aqueous solvents to infiltrate and swell the material. The shear modulus of PDMS is typically in the range of 100 kPa to 3 MPa, rendering the material flexible. The PDMS prepolymer was prepared by mixing the elastomer base and the curing agent in a proper ratio (10:1, wt/wt). The mechanical properties of the elastomer depend on this ratio.
A 10x10x2 mm 3D printed frame was placed on top of the thin film with the SRG and the pre-polymer was poured into the frame and thermally cured at room temperature for 2 days. The cured PDMS layer was removed from the thin film afterward. After the removal of the PDMS, the SRG on the thin film is intact and can be re-used multiple times.

d. Optical setup for diffraction pattern measurement
In order to characterize and check the desired photoinduced structuration on the surface of the thin film replica, a circularly polarized laser (He-Ne, 632.8nm) is used to illuminate the PDMS sample (Fig. 1). The PDMS replica of the SRG is stretched horizontally and/or vertically by a system of clamps fixed to two linear translation stages. The diffraction pattern of the sample was observed on a screen placed at 4.0 cm distance from the sample, acting as a diffuser. In order to prevent the image saturation, the central spot of the laser beam was masked via a black dot. All observations of the diffraction patterns were captured by a Canon camera (EOS 550d and Canon ultrasonic objective 28-80mm) and recorded with different exposure times for every millimeter of stretching. The unsaturated images were analyzed with the software ImageJ to get the mean position and the relative intensity of each spot of the diffraction pattern for each stretching distance. The images did not show any visible optical distortion.

e. AFM measurements

Direct measurements of the topographical characteristics, surface morphology and photoinduced modifications of the surface relief gratings were conducted using an atomic

force microscope AFM (Nano-Observer Scientec).
The topographical images were obtained at room temperature for azopolymer thin films and PDMS samples in contact and tapping mode, respectively. Images were processed with the Gwyddion free SPM data analysis software.

f. Metal dewetting process

The fabrication process is as the following: a metal film is deposited on a substrate using the PVD (Physical Vapor Deposition) techniques. The metal film thickness is 5 nm corresponding to the minimum possible thickness with the PVD process. The sample consisting of a thin silver film on the top of the nanostructure PDMS is then annealed in an electric oven at a temperature of 80°C, for two hours, corresponding to the optimized temperature and time for nanodot separation. At temperatures higher than 80°C melting of the metal surface coating leads to inhomogeneous shrinking of the metal. The result is based on the thermal dewetting mechanism. The coated metal film is then separated into many small pieces and agglomerated into small semispherical dots.

3. RESULTS AND DISCUSSION

a. Formation of quasi-crystal on azopolymer films

We create nano-cavities on an azopolymer thin film by superimposing multiple sinusoidal phase grating patterns with different directions. The different grating patterns do not interfere with each other and simply add-up on the surface of the thin film. Adding multiple sinusoidal gratings tends to smooth the surface and consequently diminish the diffraction efficiency.
It is possible to inscribe one-dimensional (1D) line gratings (fig. 2a) with varying periods through the change of the interference angle, θ, between the beams.
Following, a second illumination step was added, after rotating the samples around the surface's normal axis with an angle of 90◦, with respect to the writing beam. Such an inscription procedure resulted in a 2D cross grating with the same period, Λ, in both principal directions (fig. 2b).
A successive overwriting of multiple 1D interference patterns give rise to 2D SRGs with controlled geometries. Inscription of four SRGs by rotating the sample four times at 45◦ results in an interesting flower-like structure seen in figure 2c. Continuing a successive overwriting of eight and sixteen SRGs on the same spot by rotating the film at 22.5° and 11.25°, respectively, results in a set of complex structures seen in the figure 2d.

b. Modification of the diffraction pattern while stretching the PDMS quasi-crystal

The PDMS replica has exactly the same surface structure as the azopolymer surface. The figure 3 compares the results of diffraction intensity patterns for the azopolymer and the PDMS surfaces. We observe the same patterns in the two cases confirming that the surface topography of the azopolymer surface has been transferred on the PDMS sample. The diffraction intensity pattern could be used to monitor the evolution of the PDMS surface

structure. The figure 4 presents the evolution of the diffraction pattern of a 3-fold quasi-crystal PDMS replica under different horizontal stretching distances.
Reduction of the distance between the spots and the center of the diffraction pattern indicates a decrement in the pitch (a compression) for the sinusoidal gratings perpendicular to the stretching direction. On the contrary, the increase in the distance for the vertical spots indicates an increment (an elongation) for the sinusoidal gratings collinear to the stretching direction. Even though this is not the main point of this article, it is important to note that these transparent and stretchable quasi-crystal samples could also have interesting applications in beam steering.
The maximum of elongation without damages to the sample and without rupture of one of the holders maintaining the sample is 6 mm and corresponds to 100 % of stretching.
These elongations and compressions are linear up to six millimeters of stretching as shown in the figure 4 and the ellipticity of the diffraction pattern shows a linear relation to the horizontal stretching distance. From these measurements, we can say that a stretch at the macroscopic scale of 1 mm leads, in a nanoscopic scale, to compression of 24 nm of the pitch of the sinusoidal gratings perpendicular to the stretching direction and an elongation of 47 nm for the pitch of the sinusoidal gratings along the stretching direction.

c. Wettability tuning

We consider the PDMS samples obtained by replica of the azopolymer surface. We modified the PDMS quasi-crystal surface corresponding to the replica of a 4-fold sample by adding metallic nanoparticles in the goal to obtain a multi-scale nanoscale roughness combined with the nano- and microscopic structuration of the initial surface.
A thin, solid, homogeneous, metallic film deposited on an inert, amorphous substrate can break into droplets clusters when a sufficient activation energy is provided. We used a thermal process for breaking the metal thin film. This phenomenon, known as agglomeration or dewetting, is important in the microelectronics industry and can lead to severe drawbacks for complex systems, as it can be responsible for damages in electrical interconnections. However, we consider this drawback as an opportunity. Recently, this process was studied as one of the methods for producing arrays of nano-sized metal clusters or metal nanodot arrays, using thermal manufacturing processes, leading to agglomerated small semispherical dots [31]. These processes are based on the combination of thin metal film coatings with an optimized film thickness deposited on substrates and a thermal dewetting.
Agglomeration of metal films is a mass transport process that shrinks the thin metal film and uncovers the surface of the substrate in order to reduce the total free energy of the system. Many experimental studies have been carried out on the shrinking and agglomeration of thin metal films deposited on inert substrates [32, 33]. The PDMS material is particularly well adapted for as an inert substrate due to its main elastomeric properties.
The shrinking of the continuous edge of the dewetting film appears unaffected by the basic structural surface elements such as the surface film pattern or substrate nano-cavities at the nano-length scale of observation. The elastomer surface influences the metal film morphology in the initial growth stage of the dewetting. As a result, many random metal nanodots are generated on the substrate. The figure 5a presents the original 4-fold substrate. The figure 5b

shows the nanoparticles fabricated on the quasi-crystal surface corresponding to the 4-fold pattern sample measured with an AFM. The large depth of the nanocavities does not allow the tip to probe the bottom of all the cavities but we point out that some nucleations and growth of nanoparticles appearing in some cavities means that nanoparticles are dropped inside the nano-cavities. Figure 5c shows the distribution in size of the silver nanoparticles calculated from the AFM image. The size of the nanoparticles is uniform with a value of 25 ± 10 nm. The size distributions are measured with a grain detection after defining the threshold value. The average number of nanoparticles distributed on the surface is N = 41 nanoparticles/μm^2. The distance separating nanoparticles can be estimated with topographic measurements with an example given in figure 5d. We found an approximate distance between the nanoparticles to be about 140 ± 10 nm.

The multi-roughness and multi-scale surfaces with or without nanoparticles on the quasi-crystal structures are tested for water flow resistance. A graphical description of the surface pattern with a water droplet is given in figure 6. The wetting behavior of the samples was evaluated by contact angle measurements using the sessile drop technique via a digital microscope with a magnification range of 10x - 200x in ambient conditions. A highly pure water droplet with a volume of 10 µL was deposited on the surface and the image of the droplet was acquired with the integrated digital camera. The droplet profile was extracted and fitted through the Young–Laplace method. The contact angles between the fitted function and baseline were calculated using the ImageJ software with the associated contact angle measurement plugging that gives the contact angle value at the liquid-solid interface. For each sample, 4 drops of water were dispensed at different positions on the surface and the average value was calculated.

Since the elastomeric PDMS film can be subjected to a strain, we modify the topography of the nano and micro-scaled surface patterns using a mechanical strain. For this purpose, the PDMS sample is clamped and mechanically stretched, from 0 to 6 mm, corresponding to a stretch ratio of zero to 100 % as we defined previously. The PDMS film was mounted on a custom-designed strain stage to stretch uniaxially at different ratios. The compression is more difficult, and the maximum of compression is limited. The reason is the difficulty to constrain the sample to have a planar direction without bending or torsional variations. Moreover, PDMS films are hardly compressible (Poisson coefficient) close to 0.5.

The wettability of a water droplet is measured on different nano-engineered PDMS surfaces corresponding to 2G, 3G, and 4G, at different elongation ratios. Mechanical elongations applied to the PDMS are presented in figure 7. The increase in hydrophobicity is caused by the enhancement of the surface roughness and a higher energy is required to overcome the energetic barrier formed at the patterns. When we apply the mechanic stretching along one direction, the CA decreased as the strain increased. Upon stretching to 100%, the CA decreased to 96° from the original value of 133° for the 4G. The hydrophobicity is decreased by 8° with the reduction of the complexity of the quasi-crystal surface pattern. We note that the reduction of the hydrophobicity with the mechanical elongation is faster and with a high slope for 2G than 4G. For all the measurements there are two plateaus from 0 to 2 mm and for 4 to 6 mm. We note that the addition of nanoparticles increases the contact angles with almost 10 ° on the values of the contact angles without nanoparticles and render the surface more hydrophobic.

We suppose that when the stretching is at its maximum, the liquid fills all of the underlying structural features on the surface pattern with a complete wetting of the liquid-solid interface. This maximum stretching leads to an increase of the total wetted area.
Accordingly, tunable and reversible wetting behaviors were exhibited by various grooved quasi-crystal surfaces with different aspect ratios.
Owing to the excellent elastic recovery of PDMS films, multiple cycles of elongation and releasing were studied to satisfy the demands of practical applications. We tested the repeatability with 10 cycles, but we suppose that the number of cycles could be limited by the attachment resistance of the nanoparticles to the sample. The Young's modulus E is usually reported to be ranging from 500 kPa to 3MPa and shear modulus G from 400 kPa and 900 kPa giving it a good elasticity. The PDMS film was gradually stretched from its original length to the maximum length (100% strain) and kept at that length for an hour (insert of figure 7). Then, the strain was released and the PDMS film came back to its original length.

e. Contact angle calculation

There are two models to describe the CA on a real surface [34]. The main differences between the real surface and the ideal surface are heterogeneity and roughness. One of the two models is the Wenzel model for the chemically homogenous surface but with roughness [35].
In the Wenzel model the concept of a "roughness factor" (r) is introduced that describes the increase in surface area of a rough surface compared with the geometric area:

$$cos(\theta_w) = r.cos(\theta) \qquad (7)$$

r is always greater than 1, except in the case of a perfectly flat surface, where the actual surface and geometric surface are identical, q is the contact angle of the material without structuration.
In the other model: the Cassie–Baxter model [36], the heterogeneous and porous surface is included, and the model predicts the relationship between the contact angle and the fractional contact areas of multiple-composition surfaces. In this surface state, the air is trapped in the grooves between surface structures and forms a composite (solid/air) hydrophobic surface, resulting in a larger contact angle θ_{C-B} compared to the contact angle θ with a flat surface:

$$cos(\theta_{C\text{-}B}) = f\,cos(\theta) + f - 1 \quad (8)$$

f represents the ratio between the projected area of the solid surface in contact with the liquid over the projected total area (air and solid), corresponding to the fraction of the solid/liquid interface in the entire composite surface beneath the liquid [35, 36]. In contrast, in the Wenzel state, the liquid on the surface enters the grooves, resulting in a higher surface wettability due to the increase in the contact area.
Usually, liquids exhibit either the Cassie–Baxter wetting state or the Wenzel wetting state. We calculate the r values of the Wenzel model for all the patterned surfaces. We used the topographic images obtained by AFM measurements and we calculated the projected surface using the Matlab software. We found the following values; 2.2, 1.9, 1.8, for the 4-grating, 3-

grating, and 2-grating, respectfully. We used in the calculation the typical value of CA measured for the PDMS surface to be 106°. This value agrees with the typical values found in the literature [37]. The calculated values of θ_w equal to 111°, 109° and 108° for the 4G, 3G and 2G surfaces respectively. According to these values, we are far from the measured CA values obtained on the patterned surfaces in the condition of no stretching (fig. 7). We can conclude that this model is not able to give the measured values of the CA.

For the calculation of CA in the model of Cassie-Baxter, we consider a simple model [38 - 40] described by:

$$cos(\theta_{CB}) = \left(\frac{R}{R+d}\right)(\pi - \theta_e)cos(\theta_e) + \left(\frac{R}{R+d}\right)sin(\pi - \theta_e) - 1$$

Where, θ_e is the equilibrium contact angle of water in the air when the liquid droplet sits on the patterned surface, 2d is the distance of the separated local structures in parallel and R is the dimension of the local structure. We calculated the parameters for all the patterned surfaces. We found the CA values of 125°, 128°, 133° considering the parameters (d = 1.1 μm, R = 1.2 μm), (d = 0.8 μm, R = 0.8 μm), (d = 1.45 μm, R = 0.7 μm) for the surfaces 2G, 3G, and 4G, respectively obtained from AFM topology measurement. The obtained values by this model agrees with the measured values. In the calculations, we assumed that the θ_e is equal to 100°. We observed that the addition of nanoparticles increases the roughness. In that case, we need to include both effects of the patterned surface and the metal nanodots on the surface. A coefficient corresponding to the influence of the nanoparticles is considered in the equation of the wettability with the Cassie-Baxter model that changes the CA from 133° to 138°.

Finally, we tested the possibility of a friction that induces roll or slide for the water droplet. We rotated the support with a continuous angle from 0° to 180°. The droplet stays on the surface. For an angle of 180°, the droplet is stuck to the surface. A petal-rose effect is observed by the PDMS surface. In this position of the water droplet, we applied a mechanical elongation. The results are given in figure 8. In this experiment, we considered a 4G surface, but similar results were observed with 2G and 3G. We found a tunable and reversible wetting behavior with decreasing and increasing the degrees of patterning, as it is expected, but with a lower degree of hydrophobicity. A big CA variation is observed as a function of the stretching. For a stretching threshold of 16% the curve of the CA as a function of the stretching shows a low slope. The sensitivity of the tuning wettability is 2.5°/mm in this case. This new surface can be used for catching droplets and transferring on other surfaces [41].

4. CONCLUSIONS

We have presented the fabrication of surface quasi-crystal structures on azopolymer films and its replication through a soft lithography technique onto a transparent elastomer (PDMS). The quasi-crystal structures were prepared simply through a multistep light irradiation via an interference pattern of a laser beam without additional manipulations. The printed patterns on PDMS showed the same patterns as the masters and the same relief depths as the stamps. The light diffracted by the PDMS stamp was used to observe the deformation of the surface as a function of its stretching. This measurement was used to obtain a quantitative estimation of

the size of the nanocavities. The geometry of nanocavities for a 4-fold quasi-crystal can be estimated to be modified up to 40% of its diameter with a macroscopic stretching of the PDMS sample corresponding to 100% of the maximum elongation. A maximum stretching of 6 mm can be reached. The PDMS SRGs were used as a tailored surface for the observation of a tunable CA leading to a change of the hydrophobic conditions. The addition of nanoparticles with a metal dewetting technique increases the hydrophobic conditions of the surface. The surface becomes superhydrophobic. Finally, the rotation of the sample shows that the water droplet is stuck to the surface and that the stretching leads to a large variation of the CA.

The results presented show an interesting application of quasi-crystal replica with PDMS. The method presented here allows the fabrication of cost-effective and efficient surfaces for a super hydrophobic tunability. Several PDMS replicas (4 replicas were tested) could be fabricated with the same features without damage to the initial azopolymer film.

References

[1] Azmayesh-Fard S. M., Lam L., Melnyk A., DeCorby R. G. Design and fabrication of a planar PDMS transmission grating microspectrometer. Opt. Express 21 (2013) 11889.

[2] Gritsai Y., Goldenberg L. M., Kulikovska O., Stumpe J. 3D structures using surface relief gratings of azobenzene materials. J. of Optics A: Pure and Applied Optics 10 (2008) 125304.

[3] Yang C., Shi K., Edwards P., Liu Z. Demonstration of a PDMS based hybrid grating and Fresnel lens (G-Fresnel) device. Opt. express 18 (2010) 23529.

[4] Lee S., Jeong Y.-C., Park J.-K. Facile fabrication of close-packed microlens arrays using photoinduced surface relief structures as templates. Opt. express 15 (2007) 14550.

[5] Chen J. K., Chang C. J. Fabrications and Applications of Stimulus-Responsive Polymer Films and Patterns on Surfaces: A Review. Materials 7 (2014) 805.

[6] Vardeny Z., Nahata A., Agrawal A. Optics of photonic quasicrystals. Nature Phot. 7 (2013) 177.

[7] Gauthier R., Ivanov A. Production of quasi-crystal template patterns using a dual beam multiple exposure technique. Opt. express 12 (2004) 990.

[8] Gorkhali S. P., Qi J., Crawford G. P. Switchable quasi-crystal structures with five-, seven- and nine- fold symmetries. J. Opt. Soc. of Am. B 23 (2006) 149.

[9] Yu C., O'Brien K., Zhang Y.-H., Yu H., Jiang H., Tunable optical gratings based on buckled nanoscale thin films on transparent elastomeric substrates. Appl. Phys. Lett. 96 (2010) 041111.

[10] Hu M., Novo C., Funston A., Wang H., Staleva H., Zou S., Mulvaney P., Xia Y., Hartland G. V. Dark-field microscopy studies of single metal nanoparticles: understanding the factors that influence the linewidth of the localized surface plasmon resonance. J. of Mat. Chem. 18 (2008) 1949.

[11] Kim J. Y., Kim H., Kim B. H., Chang T., Lim J., Jin H. M., Mun J. H., Choi Y. J., Chung K., Shin J., Fan S., Kim S. Highly tunable refractive index visible-light metasurface from block copolymer self-assembly. Nature Comm. 7 (2016) 12911.

[12] Priimagi A., Shevchenko A. Azopolymer-based micro- and nanopatterning for photonic applications. J. of Polymer Sci., Part B: Polymer Physics, 52 (2014) 163.

[13] Wei R., Xu Z., Wang X. Epoxy-based azopolymer for photofabricating surface-relief quasi-crystal structures. Opt. Mat. Express 5 (2015) 1348.

[14] Liu B., Wang M., He Y., Wang X., Duplication of photoinduced azopolymer surface-relief gratings through a soft lithographic approach. Langmuir 22 (2006) 7405.

[15] Xiao J., Carlson A., Liu Z. J., Huang Y., Jiang H., Rogers J. A. Stretchable and compressible thin films of stiff materials on compliant wavy substrates. Appl. Phys. Lett. 93 (2008) 013109.

[16] Lee J. H., Ro H. W., Huang R., Lemaillet P., Germer T. A., Soles C. L., Stafford C. M. Anisotropic, hierarchical surface patterns via surface wrinkling of nanopatterned polymer films. Nano Lett. 12 (2012) 5995.

[17] J. Long, P. Fan, D. Gong, D. Jiang, H. Zhang, L. Li, M. Zhong, 'Superhydrophobic Surfaces Fabricated by Femtosecond Laser with Tunable Water Adhesion: From Lotus Leaf to Rose Petal', ACS Appl. Mater. Interfaces, 7 (2015) 9858 – 9865.

[18] J. Choi, W. Jo, S. Y. Lee, Y. S. Jung, S.-H. Kim, H.-T. Kim, 'Flexible and Robust Superomniphobic Surfaces Created by Localized Photofluidization of Azopolymer Pillars',

ACS Nano, 11 (2017) 7821−7828.
[19] Kim K. - H., Jeong Y.-C., 'One-step fabrication of hierarchical multiscale surface relief gratings by holographic lithography of azobenzene polymer', Opt. Express, 26(5) (2018) 5711 – 5723.
[20] Li Y., Dai S., John J., Carter K. R., 'Superhydrophobic Surfaces from Hierarchically Structured Wrinkled Polymers', ACS Appl. Mater. Interfaces 5 (2013) 11066−11073
[21] Barille R., Nunzi J.-M., Ahmadi-Kandjani S., Ortyl E., Kucharski S., One step inscription of surface relief microgratings. Opt. Comm., 280 1 (2007) 217-220.
[22] H. Wu**,** S. Yu, Z. Xu, B. Cao, X. Peng, Z. Zhang, G. Chai, A. Liu, Theoretical and Experimental Study of Reversible and Stable Wetting States of a Hierarchically Wrinkled Surface Tuned by Mechanical Strain. Langmuir, 3521 (2019) 6870 – 6877.
[23] Zhao S., Xia H., Wu D., Liv C., Chen Q.-D., Ariga K., Liu L.-Q., Sun H.-B. Mechanical stretch for tunable wetting from topological PDMS film. Soft Matter, 9 (2013) 4236 – 4240.
[24] Lin P.-C., Yang S., Mechanically switchable wetting on wrinkled elastomers with dual-scale roughness. Soft Matter, 5 (2009) 1011-1018.
[25] Ensikat H. J., Ditsche-Kuru P., Neinhuis C., Barthlott W., Superhydrophobicity in perfection: the outstanding properties of the lotus leaf. Beilstein J. Nanotechnol., 2 (2011) 152 – 161.
[26] Feng L., Zhang Y., Xi J., Zhu Y., Wang N., Xia F., Jiang L., Petal Effect: A Super-Hydrophobic State with High Adhesive Force. Langmuir, 2484 (2008) 114 – 4119.
[27] Bhushan B., Nosonovsky M. The rose petal effect and the modes ofsuperhydrophobicity. Phil. Trans. R. Soc. A., 368 (2010) 4713–4728.
[28] Ortyl E., Janik R., Kucharski S. Methylacrylate polymers with photochromic side chains containing heterocyclic sulfonamide substituted azobenzene. Eur. Polymer J., 38 (2002) 1871.
[29] Viswanathan N. K., Kim D. Y., Bian S., Williams J., Liu W., Li L., Samuelson L., Kumar J., Tripathy S. K., Surface relief structures on azo polymer films. J. of Mat. Chem., 9 (1999) 1941.
[30] Barrett C. J., Natansohn A. L., Rochon P. L., Mechanism of Optically Inscribed High-Efficiency Diffraction Gratings in Azo Polymer Films. J. of Phys. Chem., 100 (1996) 8836.
[31] Boragno C., Buatier de Mongeot F., Felici R., Robinson I. K., Critical thickness for the agglomeration of thin metal films. Phys. Rev. B, 79 (2009) 155443.
[32] Yoshino M., Terano M., Fabrication of Metallic Nanodot Arrays. J. of Jap. Soc. Tribologists, 63, 10 (2018) 677-683.
[33] Makarova M., Mandal S. K., Okawa Y., Aono M., Ordered monomolecular layers as a template for the regular arrangement of gold nanoparticles. Langmuir, 29 (2013) 7334.
[34]. Marmur A., Wetting on Hydrophobic Rough Surfaces: To Be Heterogeneous or Not to Be? Langmuir, 1920 (2003) 8343-8348.
[35] Wenzel R. N., Resistance of solid surfaces to wetting by water. Ind. Eng. Chem., 28, 8 (1936) 988-994.
[36] Cassie, A. B. D.; Baxter, S. Wettability of porous surfaces, Trans. Faraday Soc. 40 (1944) 546.
[37] Li X. M., Reinhoudt D., Crego-Calama M., What do we need for a superhydrophobic surface? A review on the recent progress in the preparation of superhydrophobic surfaces. Chem. Soc. Rev., 36 (2007) 1350 – 1368.

[38] Mishra H., Schrader A. M., Lee D. W., Gallo Jr. A., Chen S. -Y., Kaufman Y., Das S., Israelachvili J. N., Time-Dependent Wetting Behavior of PDMS Surfaces with Bioinspired Hierarchical Structures. ACS Appl. Mater. Interfaces. 8 (2016) 8168 – 8174.
[39] Zu Y. Q., Yan Y. Y., Single Droplet on Micro Square-Post Patterned Surfaces – Theoretical Model and Numerical Simulation. Sci. Rep. 6 (2016) 19281.
[40] Shim M. Kim H., J., Park C. H., The effects of surface energy and roughness on the hydrophobicity of woven fabrics, Textile Res. J. 84(12) (2014) 1268 – 1278.
[41] Miwa M., Nakajima A., Fujishima A., Hashimoto K., Watanabe T., Effects of the Surface Roughness on Sliding Angles of Water Droplets on Superhydrophobic Surfaces. Langmuir, 16 (2000) 5754 - 5760.

Figure Captions

Figure 1. Optical setup used to observe diffraction patterns. The samples are clamped, and a control of the stretching can be done by observing the diffraction pattern.

Figure 2. AFM surface topography measurements and the associate FFT of AFM measurements of: a) 1D or 1-fold surface grating b) 2-fold superimposed gratings, c) 16-fold quasi-crystal structure d) 32-fold quasi-crystal structure.

Figure 3. a) AFM Image of a 4-grating quasi-crystal and its PDMS replica. The mean height of the AFM sample is 32 nm. b) The comparison between the diffraction intensity patterns allows to measure the exact replication of the surface structure transfer onto the PDMS surface.

Figure 4. Evolution of the ellipticity of the central nanocavity of a 3-fold quasi-crystal SRG on PDMS with the stretch; the long axis of the ellipsoid goes from to 280 nm to 400 nm and the short axis from 320 to 260 nm. The ellipticity is measured by the observation of the optical diffraction pattern of a 3-grating quasi-crystal.

Figure 5. a) Simulation of a 4-grating surface pattern, b) AFM observation of the surface pattern covered with silver nanoparticles, c) distribution of the nanoparticle size on the surface of the sample. d) AFM topographic measurement of the sample surface.

Figure 6. Fabrication process of the surface quasi-crystal with metallic nanoparticles. a) Initial quasi-crystal surface, b) addition of nanoparticles by metal dewetting, c) final result of the pattern covered with metallic nanoparticles, d) Water droplet on the PDMS surface pattern of a 4-grating.

Figure 7. Wettability as a function of the stretching for different PDMS quasi-crystal patterns. The insert shows the reverse results as a function of different stretching cycles.

Figure 8. Wettability as a function of the stretching for a water droplet when the 4-grating quasi-crystal sample is rotated to an angle of 180°.

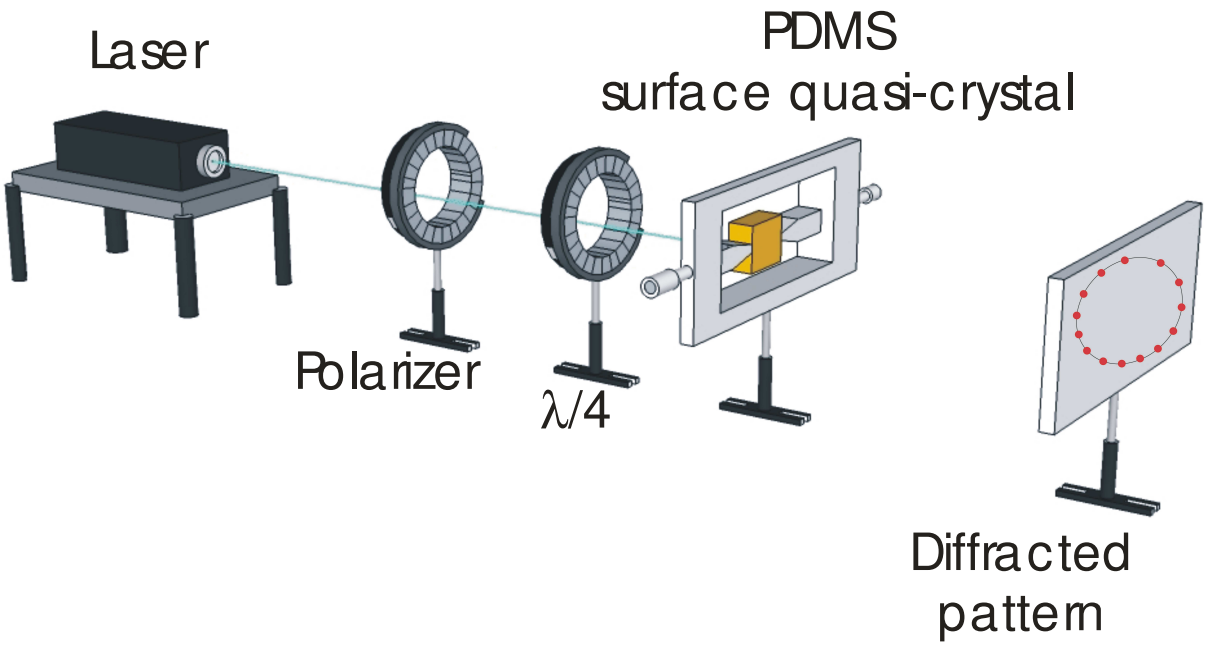
Laser
PDMS
surface quasi-crystal
Polarizer
λ/4
Diffracted
pattern

Figure 1

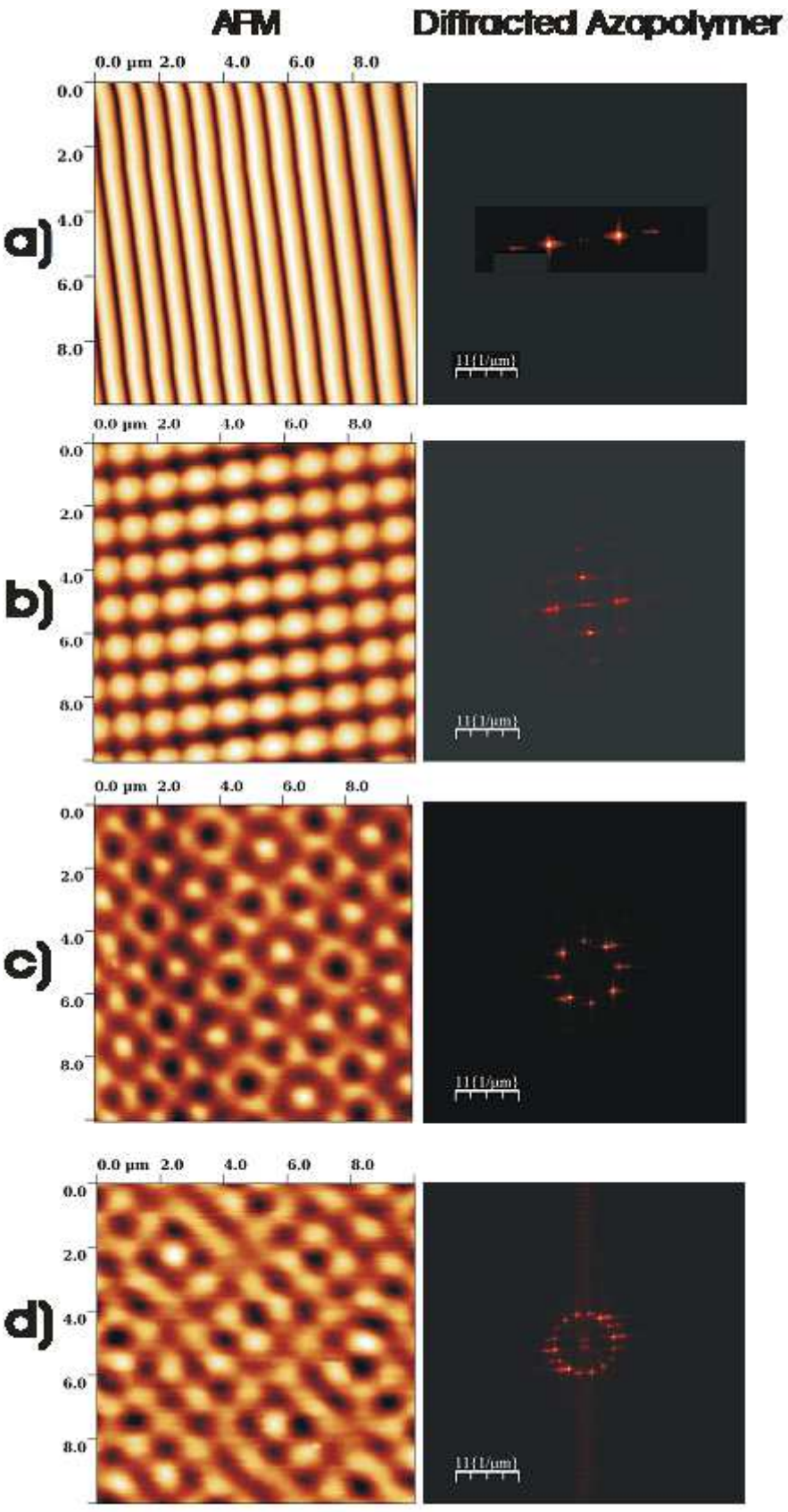
AFM
Diffracted Azopolymer
a)
b)
c)
d)
0.0 µm 2.0 4.0 6.0 8.0
0.0
2.0
4.0
6.0
8.0
1/1 (1/µm)

Figure 2

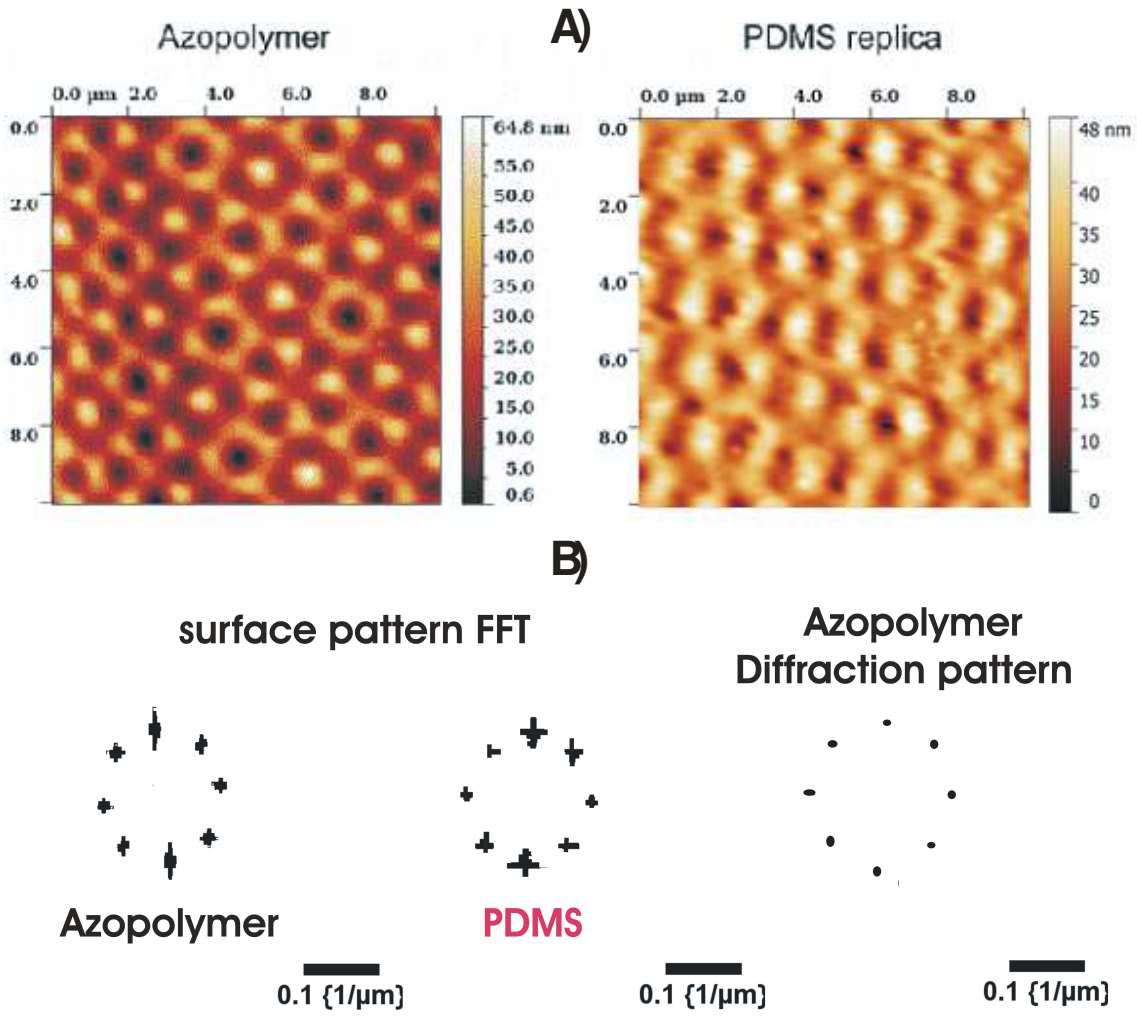
A)
Azopolymer
PDMS replica
0.0 µm 2.0 4.0 6.0 8.0
64.8 nm
55.0
50.0
45.0
40.0
35.0
30.0
25.0
20.0
15.0
10.0
5.0
0.6
48 nm
40
35
30
25
20
15
10
0
B)
surface pattern FFT
Azopolymer
Diffraction pattern
Azopolymer
PDMS
0.1 {1/µm}
0.1 {1/µm}
0.1 {1/µm}

Figure 3

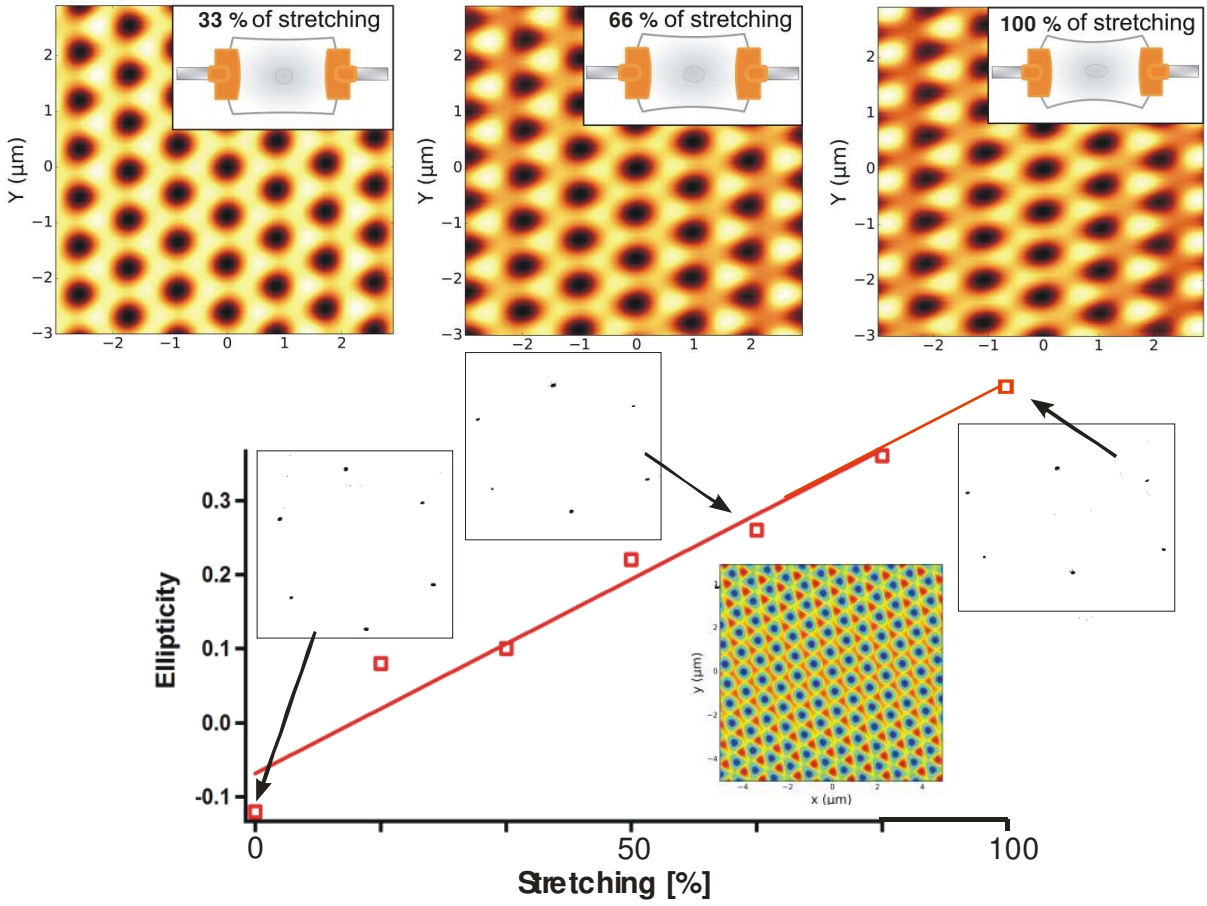
33 % of stretching
66 % of stretching
100 % of stretching
Y (µm)
Ellipticity
Stretching [%]
x (µm)
y (µm)

Figure 4

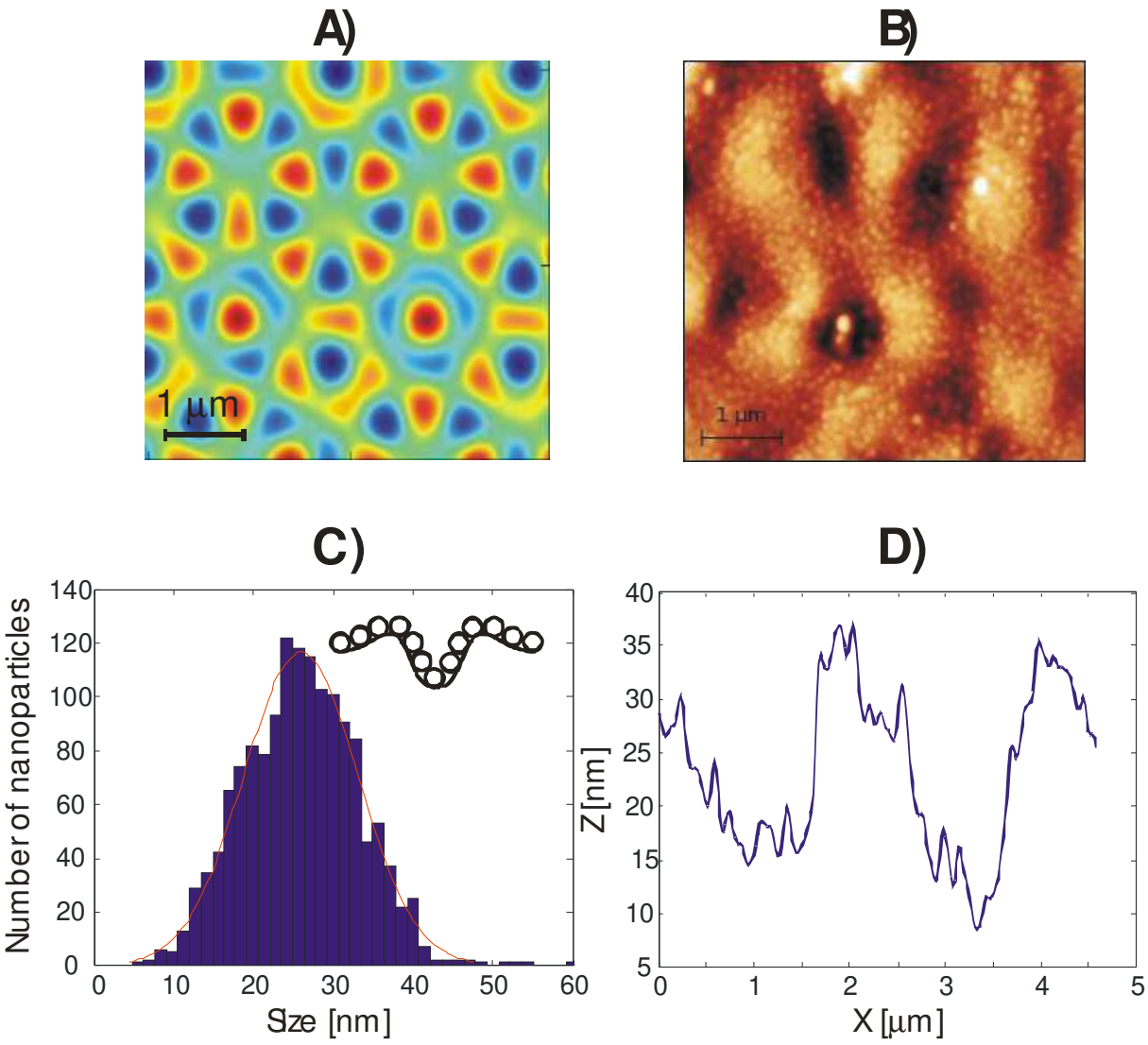
A)
B)
1 µm
1 µm
C)
D)
Number of nanoparticles
Size [nm]
Z [nm]
X [µm]
0
20
40
60
80
100
120
140
0
10
20
30
40
50
60
5
10
15
20
25
30
35
40
0
1
2
3
4
5

Figure 5

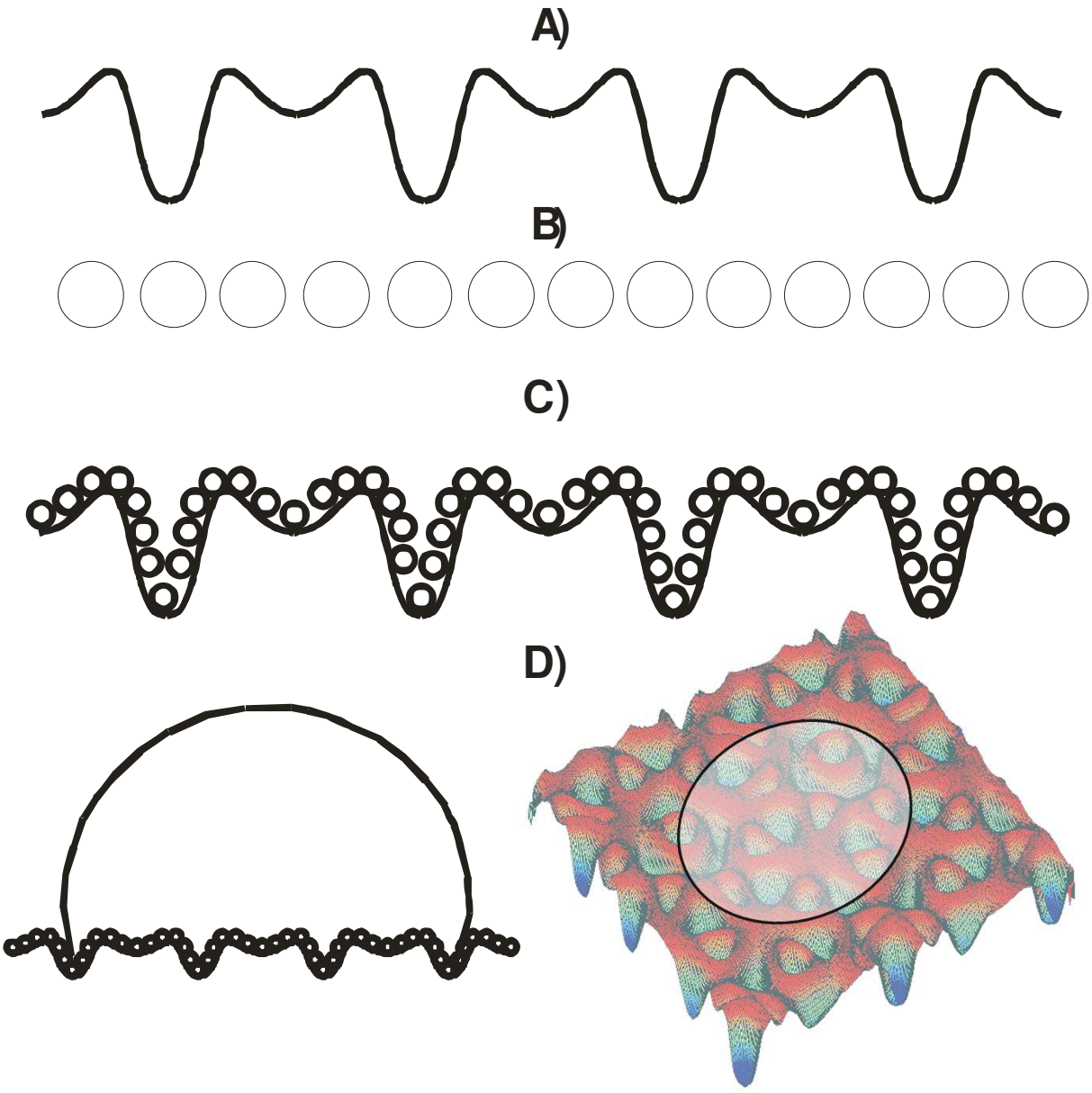

Figure 6

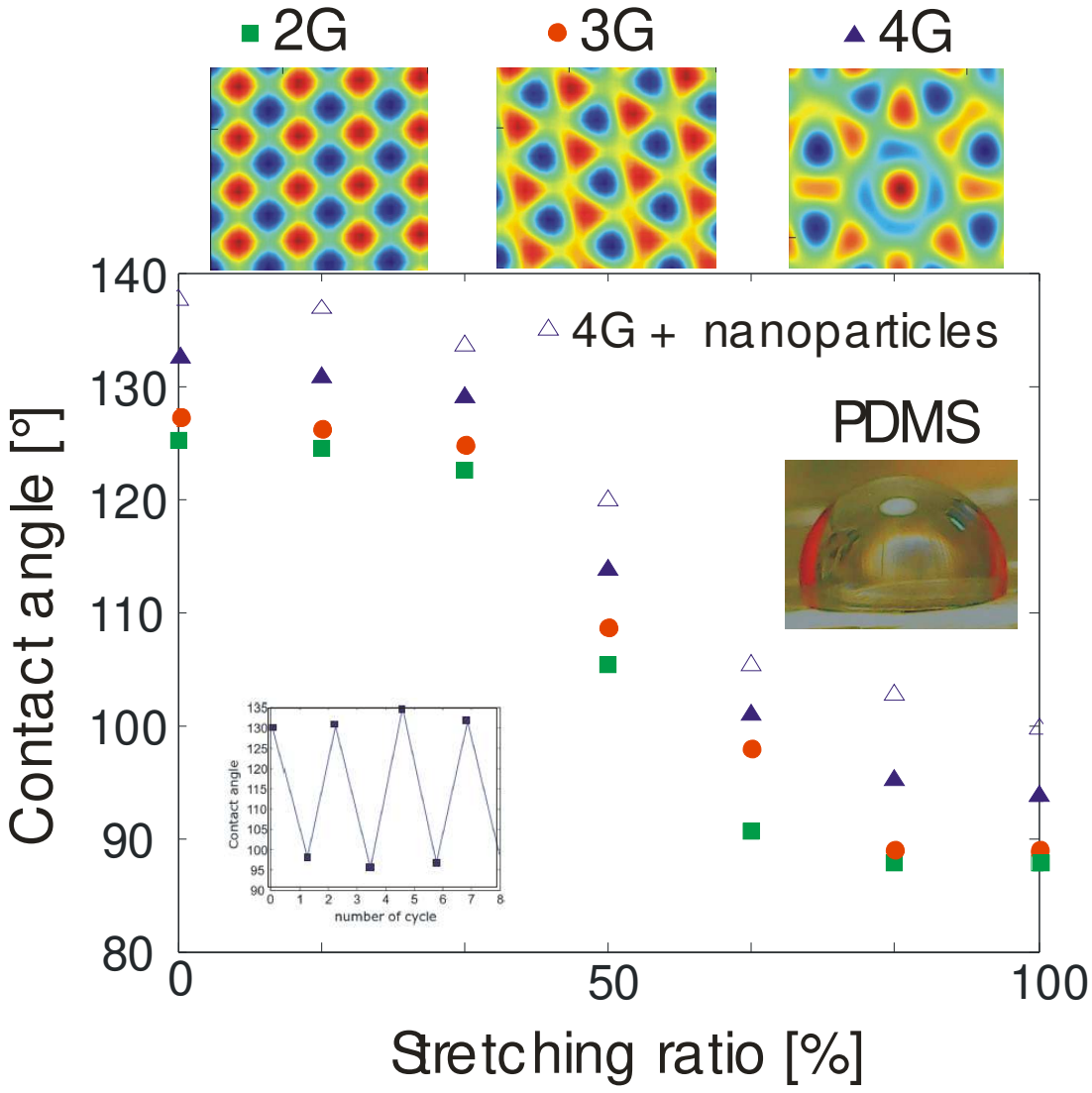
2G
3G
4G
4G + nanoparticles
PDMS
Contact angle [°]
Stretching ratio [%]
140
130
120
110
100
90
80
0
50
100
Contact angle
number of cycle

Figure 7

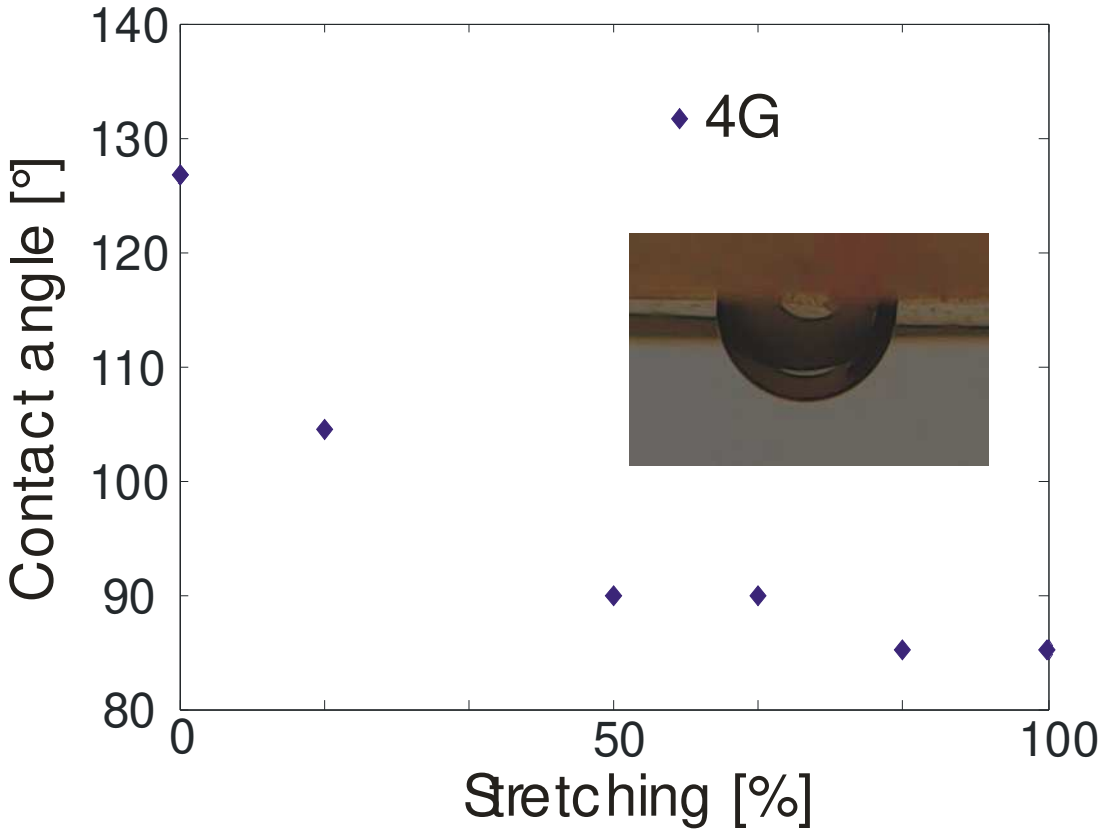

Figure 8